# Chemical Makeup and Hydrophilic Behavior of Graphene Oxide Nanoribbons after Low-Temperature Fluorination

Rebeca Romero Aburto,[†] Lawrence B. Alemany,[‡,§] Thomas K. Weldeghiorghis,[∥] Sehmus Ozden,[†] Zhiwei Peng,[‡] Aurélien Lherbier,[⊥] Andrés Rafael Botello Méndez,[⊥] Chandra Sekhar Tiwary,[†] Jaime Taha-Tijerina,[†] Zheng Yan,[‡] Mika Tabata,[†] Jean-Christophe Charlier,[⊥] James M. Tour,[†,‡] and Pulickel M. Ajayan*[,†]

[†]Department of Material Science and NanoEngineering, [‡]Department of Chemistry, and [§]Shared Equipment Authority, Rice University, Houston, Texas 77005, United States, [∥]Department of Chemistry, Louisiana State University, Baton Rouge, Louisiana 70803, United States, and [⊥]Institute of Condensed Matter and Nanosciences (IMCN), Université catholique de Louvain, Louvain-la-Neuve, 1348 Belgium

ABSTRACT
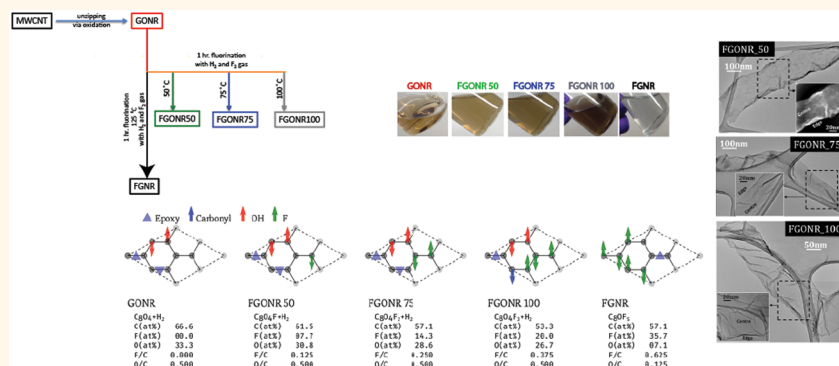
Here we investigated the fluorination of graphene oxide nanoribbons (GONRs) using H_2 and F_2 gases at low temperature, below 200 °C, with the purpose of elucidating their structure and predicting a fluorination mechanism. The importance of this study is the understanding of how fluorine functional groups are incorporated in complex structures, such as GONRs, as a function of temperature. The insight provided herein can potentially help engineer application-oriented materials for several research and industrial sectors. Direct ^{13}C pulse magic angle spinning (MAS) nuclear magnetic resonance (NMR) confirmed the presence of epoxy, hydroxyl, ester and ketone carbonyl, tertiary alkyl fluorides, as well as graphitic sp^2-hybridized carbon. Moreover, $^{19}F-^{13}C$ cross-polarization MAS NMR with ^1H and ^{19}F decoupling confirmed the presence of secondary alkyl fluoride (CF_2) groups in the fluorinated graphene oxide nanoribbon (FGONR) structures fluorinated above 50 °C. First-principles density functional theory calculations gained insight into the atomic arrangement of the most dominant chemical groups. The fluorinated GONRs present atomic fluorine percentages in the range of 6–35. Interestingly, the FGONRs synthesized up to 100 °C, with 6–19% of atomic fluorine, exhibit colloidal similar stability in aqueous environments when compared to GONRs. This colloidal stability is important because it is not common for materials with up to 19% fluorine to have a high degree of hydrophilicity.

KEYWORDS: fluorination · graphene nanoribbons · graphene oxide · fluorinated graphene · $^{19}F-^{13}C$ MAS NMR · DFT calculations

The synthesis of graphene nanoribbons (GNRs) has been widely studied[7−11] because of their great potential in various applications, such as energy-related devices,[1,2] catalysis,[3] transparent flexible touch screens,[4] gas barriers,[5] carbon fiber spinning, and coatings.[6] Among these methods, the "wet" chemistry approach starting from unzipped multiwalled carbon nanotubes (MWCNTs) is most investigated due to its production in bulk quantities and consistency. The oxidative unzipping[12,13] generates abundant oxygen-containing functionalities at both edges and basal planes, making the resulting nanoribbons highly soluble in water and polar organic solvents. The product exhibits a similar structure to graphene oxide (GO); hence,

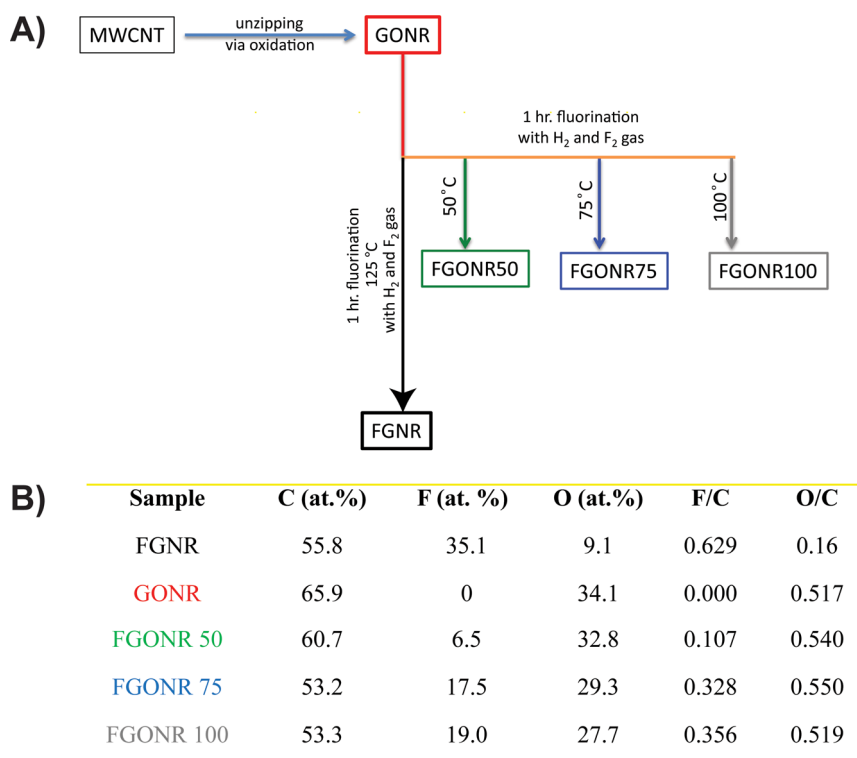| Sample	C (at.%)	F (at. %)	O (at.%)	F/C	O/C
FGNR	55.8	35.1	9.1	0.629	0.16
GONR	65.9	0	34.1	0.000	0.517
FGONR 50	60.7	6.5	32.8	0.107	0.540
FGONR 75	53.2	17.5	29.3	0.328	0.550
FGONR 100	53.3	19.0	27.7	0.356	0.519

Figure 1. Synthesis of fluorinated graphene oxide nanoribbons (FGONRs) and their XPS elemental analysis. (A) Graphical representation of the synthesis mechanism. (B) Elemental analysis of GONR, FGNR, and FGONRs 50, 75, and 100.

this material is termed graphene oxide nanoribbons (GONRs).

It is known that fluorinated graphene structures exhibit supreme hydrophobicity, enhanced thermal conductivity, as well as superior lubrication properties even at high temperatures (above 400 °C). The addition of chemical functionality can tune the degree of hydrophobicity to satisfy the needs of a particular application. There are several synthetic routes to fluorinate graphite or graphene structures.[14−17] Recently, Mathkar et al. successfully tuned the hydrophobic and amphiphobic behavior of fluorinated graphene oxide (FGO) through oxidative exfoliation of fluorinated graphite polymer, demonstrating its aqueous solubility.[18] Nevertheless, the FGO reported in Mathkar et al. had less than 7% F, which could be considered low degree fluorination. Additionally, Jankovský et al. reported the synthesis of fluorinated graphene oxide ($\leq$15% F) produced by a 6 day fluorination process (60 °C; 20% F_2/N_2 (v/v) to 3.2 bar) of GO obtained through Staudenmaier and Hummers methods.[19] The caveat of Jankovský's work could be the length of time that it takes to produce the material. Currently, fine-tuned fluorination of graphene oxide materials has not been fully achieved. Moreover, mechanistic characterization to predict a fluorination route has not been clearly elucidated. Finally, a limited amount of publications thoroughly characterize the chemical makeup of complex structures like fluorinated graphene oxides.

The purpose of this article is to generate fluorinated graphene oxide nanoribbons at low temperatures as well as to elucidate their chemical functionality and fluorination mechanism. In this work, we report a detailed chemical and physical characterization of highly fluorinated graphene oxide nanoribbons (FGONRs). To elucidate the chemical makeup of the nanoribbons, various nuclear magnetic resonance (NMR) experiments and density functional theory (DFT) calculations were used. DFT electronic structure results have been correlated with standard characterization techniques (X-ray photoelectron spectroscopy (XPS), Raman spectroscopy, Fourier transform infrared (FTIR) spectroscopy, and UV−vis absorption) to predict a fluorination mechanism. The importance of this study is the understanding of how certain functional groups appear in complex structures such as FGONR. The insight provided can potentially help engineer application-oriented materials for several research and industrial sectors.

RESULTS AND DISCUSSION

The fluorination of GONRs was conducted at four different temperatures (Figure 1A). An increase in the fluorination temperature results in a higher degree of fluorination. The objective of this paper is the further understanding of the fluorination mechanism of GONRs at low temperatures (<200 °C) by employing H_2 and F_2 gases. Furthermore, this paper seeks to determine the fluorine as well as oxygen functional
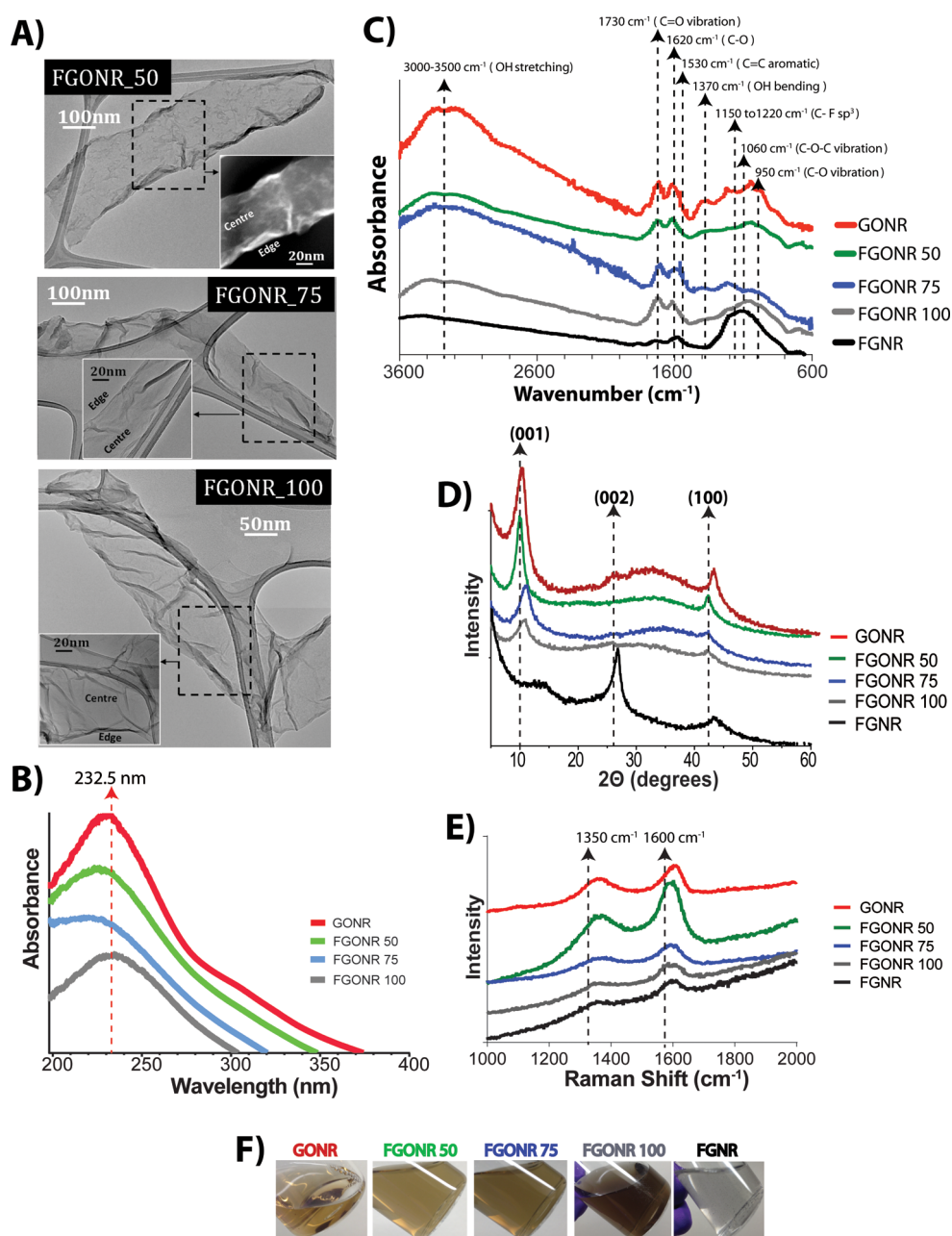
Figure 2. FGONR characterization. (A) Transmission electron microscopy image of FGONR 50, 75, and 100. (B) UV−vis spectroscopy. (C) FTIR spectroscopy. (D) X-ray diffraction. (E) Raman spectroscopy. (F) Nanoribbon's dispersivity in water; all samples have a concentration of 100 μg/mL.

groups present in graphene nanoribbons as a function of temperature. XPS elemental analysis performed on the nanoribbons exhibits fluorine percentages ranging from 6.5 to 35 and oxygen from 9 to 34 (Figure 1B).

Extensive characterization of these nanoribbons was conducted to determine if any morphological or chemical changes occurred due to the different synthetic routes. Interestingly, it was observed that the degree of buckling in the center of the ribbons increased as a function of temperature (Figure 2A). FGNRs prepared at 125 °C showed the highest buckling behavior (Supporting Information Figure S1).

Fluorinated graphene is known to be hydrophobic due to the low surface energy of the CF bond.[18,20] However, when oxygen functional groups are present, a hydrophobic to hydrophilic transition can occur.

Further chemical functionalization often produces different electronic transitions; as a result, a shift in the absorption spectrum of each sample can be detected. To determine if a shift occurs on the FGONR samples compared to the GONRs, absorption spectra in the ultraviolet to visible (UV−vis) range were obtained (Figure 2B). GONRs present a peak maximum at a wavelength of 232 nm and a shoulder around

300 nm. FGONRs 50 and 75 blue shift to values around 220 nm, while FGONR 100 red shifts and presents a peak maximum around 234 nm. It can be concluded that FGONRs 50 and 75 could have a slightly higher number of excited π bonding electrons when compared to those present in GONR and FGONR 100. Overall, the absorbance wavelength for the nanoribbons is in the range of graphene oxide (GO). To conduct the spectroscopic measurements mentioned above, all materials (GONRs, FGONRs) were dispersed in water and presented good colloidal stability, with minimum sedimentation for at least 2 months (Figure 2F). The ζ-potential of GONR and FGONRs 50, 75, and 100 resulted in negative values of 38, 30, 29, and 32 mV, respectively. Therefore, the nanoribbons are negatively charged under a 6.6 pH aqueous environment. Hydrophobic FGNRs failed to produce a stable colloidal solution in water.

Initially, to determine some of the functional groups present in the nanoribbons, FTIR spectra were obtained (Figure 2C). GONRs present several oxygen functionalities that are in agreement with those seen in GO.[21] The C—O and C—O—C vibrations as well as the OH bending and stretching in the GONR spectrum get transformed into broad diminished peaks as the fluorination temperature increases, resulting in the FGONR (50, 75, 100) samples. FGNR shows minimal absorbance from those oxygen functional groups. Inversely, as the fluorination temperature increases from 50 to 125 °C, the tertiary alkyl fluoride (CF) peak absorbance (1150 to 1220 cm^{-1}) intensifies. The signals from FGONR and FGNR are in agreement with what has been reported for fluorinated graphene (FG) and fluorinated graphene oxide (FGO) structures.[22,23]

Intuitively, the reduction of oxygen groups as the temperature increases can result in a decrease in interlayer spacing. Therefore, XRD characterization is required to determine if this indeed happens and between which temperature regimes the transition is observed (Figure 2D). GONRs and FGONR 50 present the highest d_{001} plane spacing ($\sim$8.8 Å), followed by FGONRs 75 and 100 with a d_{001} plane spacing on the order of $\sim$7.8 Å. Finally, FGNR presents the smallest d_{001} plane spacing ($\sim$7.2 Å). However, compared to the d_{001} plane spacing of graphene ($\sim$3.36 Å), FGNR d_{001} interlayer spacing increases by 2.1-fold. This perpendicular expansion with respect to the basal plane is expected due to the fluorine functional groups in the structure and lies within the range of reported values.[16,19,24,25]

Pristine graphene is composed almost exclusively of sp^2-hybridized carbons. Once defects such as vacancies or functional groups are added to the structure, some of the carbons will present an sp^3-hybridization. The hybridization state will influence the optical and conductive properties of the material, favoring a metal-to-insulator transition if the D/G band ratio tends

to unity. Due to the fluorine and oxygen functionalization, the D mode ($\sim$1350 cm^{-1}) peak broadens as the fluorination progresses from GONR to FGNR (Figure 2E). The G mode ($\sim$1600 cm^{-1}) provides information on the stretching of the C—C bond in graphitic materials. When this peak is narrow, the sample is similar to pristine graphene. However, when the G mode peak broadens, this could indicate in-plane buckling in the structure. From these results, we should expect buckling or puckering in the nanoribbons. The buckling can be confirmed by the micrographs presented in Figure 2A and Supporting Information Figure S1. Overall, the D/G ratio for GONR and FGONRs is similar (0.6 to 0.68), perhaps because of the high degree of functionalization (Figure 2E). In the case of FGNR (Figure 2E), the ratio is higher (0.82) and it could be attributed to higher content of sp^3-hybridized carbons in the structure due to the significant amount of fluorine added (Figure 1B).

To confirm the presence of the functional groups detected by FTIR spectroscopy, XPS spectra were obtained on all samples (Figure 3). With regard to the oxygen functionalities, the XPS results are in agreement with the trend observed through FTIR spectroscopy. Interestingly enough, for fluorine groups, XPS gave an indication of not only CF but also CF$_2$ groups in the FGONRs 75 (Figure 3D) and 100 (Figure 3E) and FGNR (Figure 3B) samples. As expected, GONRs only presented signals consistent with oxygen functionalities and sp^2-hybridized carbon (Figure 3A).

Due to the indication that CF and CF$_2$ fluorine groups could be present in the FGONRs and FGNR samples, direct ^{13}C pulse MAS NMR spectra were obtained on each sample. The GONR spectrum (Figure 4A) is similar to that of graphene oxide.[21,27] As expected, the spectrum shows three signals at about 60, 70, and 130 ppm, corresponding to epoxy, hydroxyl, and graphitic sp^2 carbon functionalities, respectively. As expected, the epoxy and graphitic sp^2 carbon signals in the direct ^{13}C pulse spectrum are proportionately stronger than that in a ^{1}H—^{13}C cross-polarization spectrum. Relatively strong signals can also be observed from ester carbonyl (170 ppm) and ketone carbonyl (190 ppm) functional groups (Figure 4A). The lactol group signal near 100 ppm appears similar in intensity compared to the spectrum reported by Gao et al.[21,27] The increase in ketone and ester carbonyl may result from an enhancement regarding edge reactivity of the ribbons *versus* the edge reactivity in graphene or graphite. However, the evaluation of the edge reactivity in these samples is beyond the scope of this work.

In comparison, the direct ^{13}C pulse FGNR spectrum (Figure 4B) shows two characteristic signals with maxima at 88 and 128 ppm, attributed to CF of sp^3-hybridized carbon and graphitic sp^2 carbon, respectively. Lengthening the relaxation delay from 20 to 60 s had a negligible effect on the absolute and
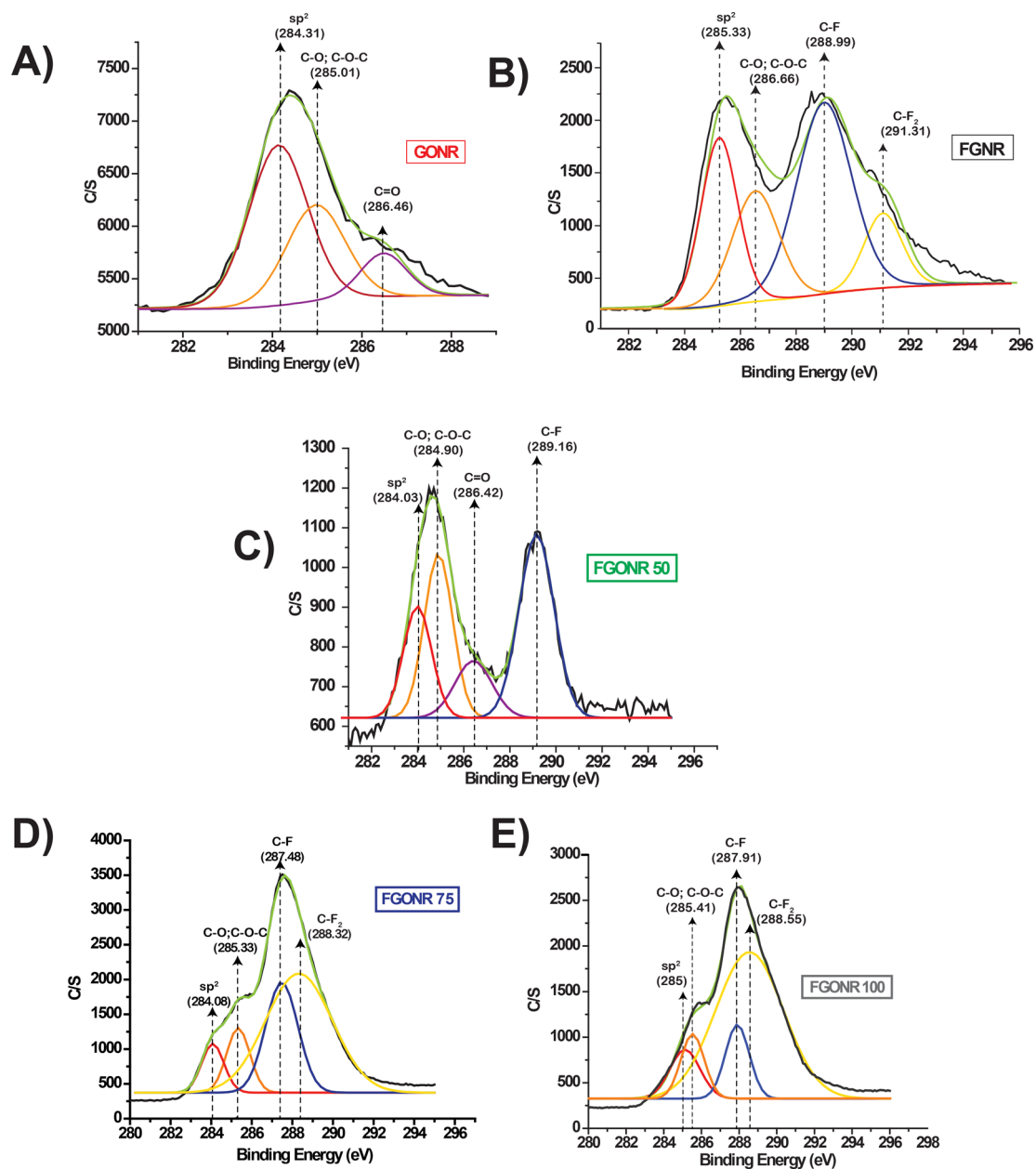
Figure 3. X-ray photoelectron spectroscopy. (A) GONR. (B) FGNR. (C) FGONR 50. (D) FGONR 75. (E) FGONR 100. The functional group binding energies are C−F (288−290 eV); C=O (285−286 eV); C−O; C−O−C (285−287 eV); sp^2 (284−285 eV). The peak located at ~290 eV could indicate the presence of CF$_2$ groups in the nanoribbons.[26]

relative intensities of the signals. The signal corresponding to graphitic sp^2 carbon exhibits a significant upfield skew (Figure 4B) that may result from CF$_2$ functional groups, which commonly give a signal around 111 ppm in fluorinated carbonaceous materials (additional details are in the Supporting Information). While looking at the XPS characterization of FGNR, FGONR 75, and FGONR 100 (Figure 3B,D,E), we see that there is a peak around 290 eV, indicative of CF$_2$ groups.[26]

The direct ^{13}C pulse FGONR 50 spectrum (Figure 4C) shows a decreased signal in the region corresponding to epoxy (60 ppm), hydroxyl (70 ppm), and graphitic sp^2 carbon (130 ppm) compared to the corresponding

GONR spectrum (Figure 4A). Because of the low extent of fluorination of FGONR 50 (Figure 1B), signals for CF and CF$_2$ are not readily obvious; the XPS spectrum (Figure 3C) is a much better indicator of the presence of CF and the apparently negligible presence of CF$_2$.

The direct ^{13}C pulse FGONR 75 spectrum (Figure 4D) indicates that even fewer epoxy and hydroxyl groups are present, while the intensity is clearly greater in the region that can result from CF, lactol, and CF$_2$ signals. The XPS spectrum (Figure 3D) indicates the presence of CF$_2$ as well as CF groups. Graphitic and ester carbonyl signals are clearly recognizable in the NMR spectrum. Overall, the NMR spectrum indicates that FGONR 75 has a very complex structure.
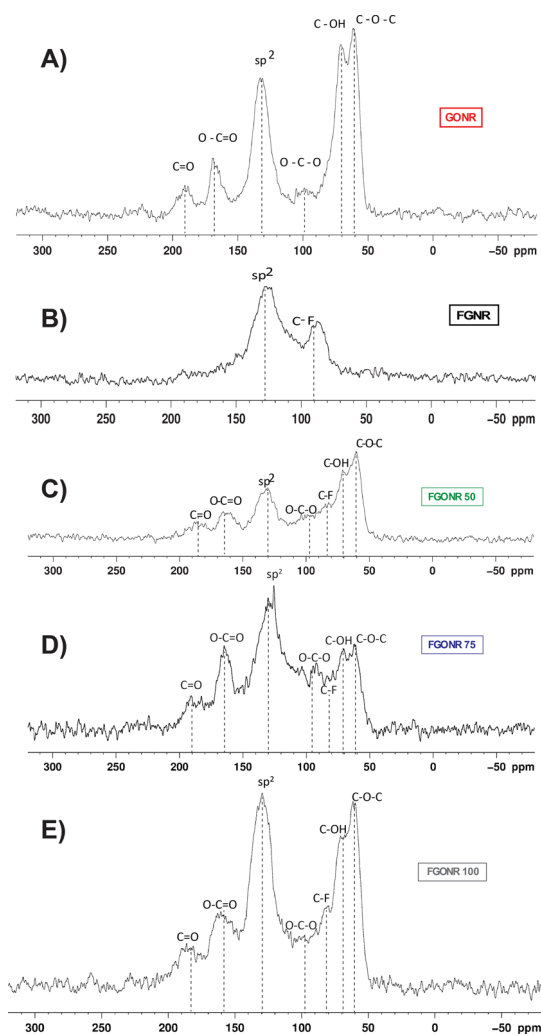
Figure 4. Direct ^{13}C pulse MAS NMR spectra of GONR, FGNR, and FGONR fluorinated at 50, 75, and 100 °C. All spectra were acquired with a 20 s relaxation delay, with the FIDs processed with 50 Hz (1 ppm) of line broadening. (A) GONR spectrum: 12 kHz MAS, 41 ms FID, 4400 scans. (B) FGNR spectrum: 15 kHz MAS, 20.5 ms FID, 4400 scans. (C) FGONR 50 spectrum: 15 kHz MAS, 41 ms FID, 4400 scans. (D) FGONR 75 spectrum: 15 kHz MAS, 41 ms FID, 20,000 scans (limited amount of material). (E) FGONR 100 spectrum: 15 kHz MAS, 41 ms FID, 4400 scans.

The direct ^{13}C pulse FGONR 100 spectrum (Figure 4E) is more similar to the spectrum of FGONR 50 than to the spectrum of FGONR 75, even though only relatively small changes are observed in the elemental composition of FGONR 100 compared to that of FGONR 75 (Figure 1B). However, the XPS spectrum of FGONR 100 (Figure 3E) suggests that CF_2 groups are much more prevalent than CF groups compared to FGONR 75.

Although much less common than $^{1}H-^{13}C$ cross-polarization, $^{19}F-^{13}C$ cross-polarization has been used to study a wide range of fluorinated materials (see the Supporting Information). Obtaining ^{13}C spectra via $^{19}F-^{13}C$ cross-polarization with a short contact time appeared to be the best approach for unambiguously demonstrating the presence of CF and, especially, CF_2 groups in the FGNR and FGONR materials. Using a short
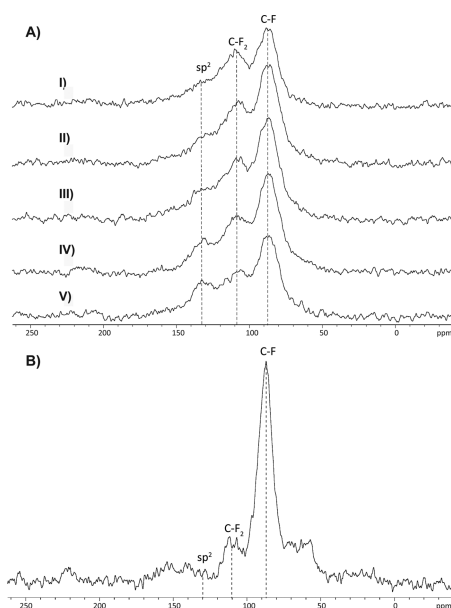

Figure 5. $^{19}F-^{13}C$ CPMAS NMR spectra of FGNR and FGONR 50. (A) FGNR spectra obtained with a contact time t_{cp} of (I) 0.5 ms, (II) 1.0 ms, (III) 1.5 ms, (IV) 2.0 ms, and (V) 3.0 ms. Spectra were obtained with 12 kHz MAS, a 3 s relaxation delay, and 20000 scans (except for the spectrum obtained with t_{cp} = 0.5 ms, where 40000 scans were acquired). (B) Spectrum of FGONR 50 obtained with a contact time of 0.5 ms, 12 kHz MAS, a 3 s relaxation delay, and 40960 scans.

contact time results in preferential detection of carbons with directly bound fluorine. This cross-polarization approach also appeared to be more unbiased than deconvoluting complex spectra to establish the presence of fluorine groups.[28] Indeed, $^{19}F-^{13}C$ CP experiments performed with multiple contact times have been used to study a wide variety of materials;[29−40] of the materials studied this way, graphite hydrofluoride[29] is perhaps the most similar to the FGNR and FGONR materials in this report.

The spectra from a series of $^{19}F-^{13}C$ CP experiments on FGNR with contact times ranging from 0.5 to 3.0 ms are shown in Figure 5A. The signals slightly upfield of 90 ppm result from CF groups, while the signals at about 110 ppm are clearly consistent with CF_2 groups. The CF_2 signals are particularly noticeable at the shortest contact times. As the contact time is lengthened, a signal at about 130 ppm emerges from the long-range cross-polarization of (nonfluorinated) graphitic sp^2 carbons, for which the $^{19}F-^{13}C$ dipole−dipole interaction is much weaker.

The CP results establish that the upfield skew of the graphitic sp^2 carbon signal in the direct ^{13}C pulse spectrum of FGNR (Figure 4B) results from CF_2 groups. The peak maximum at 128 ppm in the direct ^{13}C pulse spectrum is proportionately much stronger than the corresponding signal in the CP spectrum obtained with t_{cp} = 3.0 ms (Figure 5A) because all the aromatic carbons can be detected in the direct ^{13}C pulse experiment, while only the aromatic carbons

A) ▲ Epoxy ↕ Carbonyl ↑ OH ↑ F

GONR
$C_8O_4+H_2$
C(at%)	66.6
F(at%)	00.0
O(at%)	33.3
F/C	0.000
O/C	0.500

FGONR 50
$C_8O_4F+H_2$
C(at%)	61.5
F(at%)	07.7
O(at%)	30.8
F/C	0.125
O/C	0.500

FGONR 75
$C_8O_4F_2+H_2$
C(at%)	57.1
F(at%)	14.3
O(at%)	28.6
F/C	0.250
O/C	0.500

FGONR 100
$C_8O_4F_3+H_2$
C(at%)	53.3
F(at%)	20.0
O(at%)	26.7
F/C	0.375
O/C	0.500

FGNR
C_8OF_5
C(at%)	57.1
F(at%)	35.7
O(at%)	07.1
F/C	0.625
O/C	0.125

B) Radial Distribution Function (a.u.) — Total ▮ C−C ▮ C−O ▮ C−F

C) Density of States (a.u.)
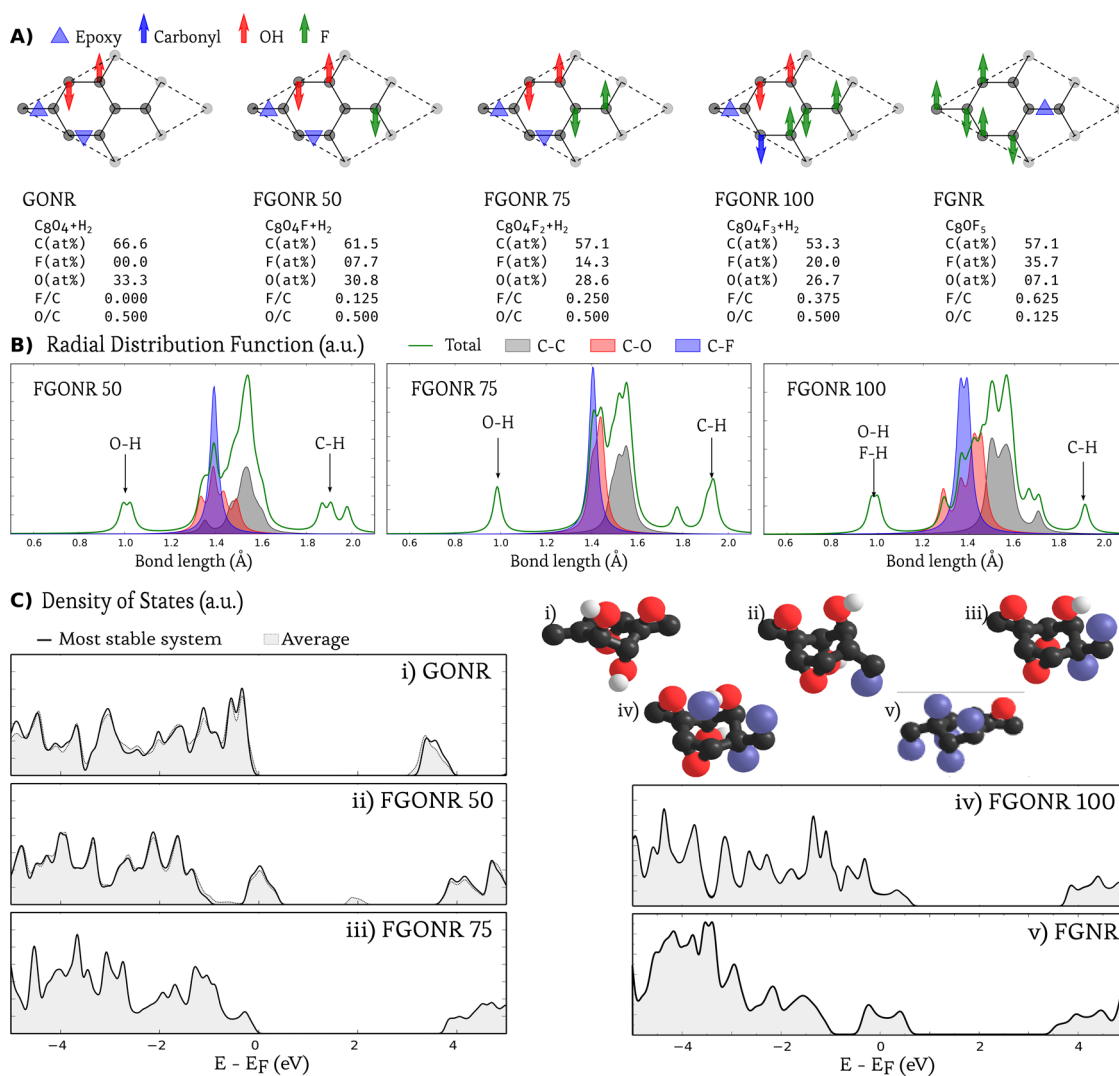— Most stable system ▮ Average

Figure 6. Schematic representation of the most stable models for GONR, FGONR (50, 75, 100), and FGNR, their corresponding stoichiometry, and density of states in a 2 × 2 graphene cell. (A) Epoxy, hydroxyl, ketone carbonyl, and fluorine groups are represented by a blue triangle and a red, blue, and green arrow, respectively. The direction of the triangle or the arrow indicates the position below or above the graphene plane. (B) Radial distribution functions for the FGONRs highlight the contributions of C−C, C−O, and C−F bonds in the various models. (C) Density of states of the most stable system (black curve) for the different models of GONR, FGONR (50, 75, 100), and FGNR and the weighted average (shaded area) of all the considered atomic configurations.

spatially near fluorine can be detected in the CP experiment.

The relative intensity of the CF_2 signal in the CP spectra clearly decreases as the contact time increases (Figure 5A). The ^{19}F spin−lattice relaxation time in the rotating frame appears to be significantly shorter for CF_2 than for CF.

The [19]F−[13]C CP spectrum of FGONR 50 obtained with t_{cp} = 0.5 ms is dominated by a signal from CF groups; much weaker signals consistent with CF_2 groups and epoxy and hydroxyl groups are also evident (Figure 5B). Since the sample contains relatively little fluorine (Figure 1B) and since the epoxy and hydroxyl signals are generated by much weaker, long-range [19]F−[13]C dipole−dipole interactions, the CF_2 content is very low (consistent with the XPS data, Figure 3C).

To further understand the structural, chemical, and electronic properties of FGONRs, total energy DFT calculations were performed.[41] The treatment of defects is often a challenge in either the periodic boundary condition or in the isolated system approaches commonly used in *ab initio* techniques. For small concentration of defects, both approaches require the consideration of large systems. In this case, however, the concentrations are rather high, leaving room for some approximations. A close examination of the stoichiometry of chemical species given in Figure 1B suggests an atomic model based on a 2 × 2 graphene cell (8 C atoms). Within such assumption, the FGNR can be modeled with 14 atoms [C_8OF_5], the GONR with 12 atoms [C_8O_4], and the FGONR (50, 75, 100) with 13, 14, and 15 atoms

$[C_8O_4F_{(1,2,3)}]$, respectively (see Figure 6A, top panel). Since hydrogen atoms are not quantifiable from experiments, they are ignored in the stoichiometry calculation. Note that, according to the XPS and NMR results presented above, only the most common oxygen functional groups, namely, epoxy and hydroxyl, have been considered. In addition, the CF_2 contributions are assumed to be present only at the edges of the nanoribbons. Finally, for high concentrations of fluorine, a ketone carbonyl group sometimes appears after structural relaxation. Nevertheless, the agreement with Figure 1B suggests that, *on average*, the local atomic structure indeed follows the stoichiometry considered in these models.

Total energy DFT calculations were performed to discover the most stable structures among more than 80 different atomic models of various stoichiometries, to analyze their geometries and elucidate some patterns (see Supporting Information Figures S4 and S5). A few general rules can be extracted from our simulations. In GONRs, an increase of stability is observed when epoxy groups are equally located on both sides of the graphene plane. The situation is similar for hydroxyl groups, although they tend to be on the opposite side with respect to the closest epoxy group. This result is in agreement with recent *ab intio* calculations performed on graphene oxide models.[42] Following these heuristics, the first added F atom prefers to lie on top of a carbon atom either on the opposite side to the closest epoxy or on the opposite side of the closest hydroxyl. When two F atoms are added, the most stable case is found with each of them on opposite sides of the graphene plane and one of them on the opposite side of the hydroxyl. Adding more F atoms often results in the formation of HF, which desorbs, except when the F atom is bound underneath a carbon, which forms part of an epoxy group, resulting in a ketone carbonyl group (creation of a C—F bond). However, this is counterbalanced with the fact that, at higher temperatures where the $C_8O_4F_3$ is expected, the hydroxyl species decompose. Several models of GONRs containing only epoxy groups were also investigated and can be found in the Supporting Information. The distribution of C—C, C—O, and C—F bond lengths is analyzed *via* the radial distribution function (RDF) (also called pair correlation function), which is presented in Figure 6A.

In GONRs and FGNRs, the C—C bond length is found to be ~1.50 Å, which is much larger than that in pristine graphene (1.42 Å). Such bond length increase could be attributed to the lattice expansion. In FGONRs, the RDF related to the C—C bond is more broadened and sometimes exhibits a multipeak structure with shorter bond lengths. The C—O bond length is centered around 1.42 Å in GONRs, and as for the C—C bonds, it tends to be shifted to smaller values and be split as the

concentration of fluorine increases. Finally, the C—F bond length is found to be almost constant with a value of 1.40 Å.

The densities of states of the most stable atomic structures and of the weighted average of other stable configurations have been computed for various stoichiometries and are presented in Figure 6B. The most stable configuration of GONR structures exhibits a semiconducting behavior with a band gap (E_g) of ~3.0 eV. Note that band gaps as well as the dispersion of the conduction bands are usually underestimated at the DFT ground-state level. Nevertheless, this result is in agreement with the almost transparent aspect of the GONRs, as illustrated in Figure 2F. For FGONR 50, the most stable configuration exhibits states close to the Fermi energy, inducing a metallic behavior. FGONR 50 will thus absorb visible light. In addition, there is an energy band gap just after this set of states, but conduction states generally reappear at higher energy (ca. 3.5 eV) as in GONR, which qualitatively explains the absorption in the UV spectra around 230 nm (Figure 2B). The most stable FGONR 75 structures are not found to be metallic. This semiconducting behavior might be explained by a higher symmetry of the atomic structure of our model, which is probably an artifact of the supercell approach. Nevertheless, states around the Fermi energy are clearly observed for FGONR 75 using atomic models containing only epoxy groups (see Supporting Information). Finally, the most stable atomic structure for the FGONR 100 model is also found to be metallic. When using only epoxy groups, the electronic structure of FGONR 100 is characterized by a strong peak at the Fermi level and the absence of a band gap at higher energies, thus explaining the strong absorption of the visible light as observed in Figure 2F.

CONCLUSION

In conclusion, low-temperature fluorination of GONRs has been possible due to the reactivity of the H_2 and F_2 gas mixture. Additionally, this process has been shown to be temperature-dependent. Interestingly, the tertiary alkyl fluoride (CF) groups appear at the lowest fluorination (50 °C), while the secondary alkyl fluoride (CF_2) groups appear at a higher temperature. Perhaps the fluorination mechanism can be explained by the development of CF groups at the center of the structure followed by CF_2 at the edges of the structure as the fluorination temperature increases. FGONRs have complex chemical structures, but this study has unambiguously characterized these structures and its fluorination mechanism. Fluorinated graphene oxide nanoribbons exhibit enhanced aqueous solubility even at high atomic fluorine percentages (19%). This work provides insight into the fluorination mechanism of fluorinated graphene

oxide nanoribbons and their temperature dependency. Furthermore, functional group tuning could broaden the technological horizon of these graphene materials.

METHODS

Nanoribbon Synthesis. GONRs were made according to the method described in Marcano et al.[11] and Higginbotham et al.[13] Briefly, 150 mg of MWCNTs was suspended in 36 mL of H_2SO_4 by stirring the mixture for a period of 1 h. H_3PO_4 (85%, 4 mL) was then added, and the mixture was allowed to stir another 15 min and heated to 65 °C. $KMnO_4$ (900 mg) was then added to the solution, and the reaction was conducted for 10 h. After that, the reaction was cooled to room temperature and poured onto ice (~80 mL) with 30% H_2O_2 (3 mL). For workup, the solution was centrifuged (4000 rpm for 4 h), and the supernatant was decanted away. The remaining solid material was then washed in succession with 40 mL of water, 40 mL of 30% HCl, and 40 mL of ethanol (2×); for each wash, the solution was centrifuged (4000 rpm for 4 h) and the supernatant decanted away. The material remaining after this extended multiple-wash process was coagulated with 200 mL of ether, and the resulting suspension was filtered over a PTFE membrane with a 0.45 μm pore size. The solid obtained on the filter was vacuum-dried overnight at room temperature, obtaining ~105 mg of product.

FGNRs were synthesized via a homemade fluorination reactor. The GONR sample was sealed in the reactor and pumped down to 0.400 Torr. Then, the reactor was filled with Ar to ambient pressure and heated to 125 °C. When the temperature was stabilized, the gas flow was changed to 10 sccm of H_2 and 15 sccm of F_2, and the fluorination reaction lasted for 1 h. After the reaction, the sample was allowed to cool in Ar for approximately 30 min before taking it out from the reactor.

FGONRs were synthesized via a homemade fluorination reactor. The GONR sample was sealed in the reactor and pumped down to 0.400 Torr. Then, the reactor was filled with Ar to ambient pressure and heated to a certain temperature (50, 75, and 100 °C). When the temperature was stabilized, the gas flow was changed to 10 sccm of H_2 and 15 sccm of F_2, and the fluorination reaction lasted for 1 h. After the reaction, the sample was allowed to cool in Ar for approximately 30 min before taking it out from the reactor.

Nuclear Magnetic Resonance. Direct ^{13}C pulse MAS NMR spectra were obtained on a Bruker Avance III, two-channel spectrometer with a 4.7 T magnet (50.3 MHz ^{13}C, 200.1 MHz ^{1}H) with 12–15 kHz MAS of 4 mm outer diameter rotors and ^{1}H decoupling during ^{13}C FID acquisition. Previous work has shown that such spinning significantly averages [13]C–[19]F dipole–dipole broadening in CF groups.[18,43] [13]C chemical shifts are relative to glycine carbonyl defined as 176.46 ppm.[44] ^{19}F–^{13}C CPMAS NMR spectra were obtained on a Bruker Avance three-channel spectrometer with a 9.4 T magnet (100.6 MHz ^{13}C, 376.4 MHz ^{19}F, 400.1 MHz ^{1}H) with 12 kHz MAS of 4 mm outer diameter rotors and simultaneous ^{1}H and ^{19}F decoupling during ^{13}C FID acquisition. (The ^{19}F decoupler offset was approximately in the middle of the CF and CF_2 ^{19}F signals, with 70 kHz ^{19}F decoupling power.) Under these conditions, the Kel-F [poly(chlorotrifluoroethylene)] rotor caps do not give a signal. [13]C chemical shifts are relative to adamantane CH defined as 38.48 ppm.

Density Functional Theory Calculations. Total energy DFT calculations were performed using a numerical linear combination of atomic orbitals as implemented in the Siesta package.[41] The generalized gradient approximation for the exchange correlation functional using norm-conserving pseudopotentials and double-ζ basis sets were used to expand the wave functions. The energy levels are populated using a Fermi−Dirac distribution with an electronic temperature of 250 K, and an energy cutoff of 500 Ry is used. A 45 × 45 Monkhorst−Pack grid was used for the integration of the 2D Brillouin zone. The geometries are fully relaxed until the forces on each atom and stress tolerance are less than 0.005 eV/Å and 0.001 GPa, respectively.

For each stoichiometry, the number of equivalent configurations that can be constructed is given by the combination of the number of additional dopants and the available sites. To avoid the calculation of this rapidly increasing number of configurations, total energies were computed from DFT at each step. Only the most stable configurations (E_0) were considered in the subsequent steps. The discrimination of the less stable structures is based on the difference in total energy between these configurations ($DE_i = |E_0 - E_i|$), within the Boltzmann distribution ($\exp(-bDE_i)$, with $b = 1/k_BT$ and $T = 400$ K). Similarly, the average RDF and the density of states were computed taking into account the Boltzmann distribution. Except for few cases, the distribution is dominated by the most stable structure.

Conflict of Interest: The authors declare no competing financial interest.

REFERENCES AND NOTES

1. Zhang, C.; Peng, Z.; Lin, J.; Zhu, Y.; Ruan, G.; Hwang, C.-C.; Lu, W.; Hauge, R. H.; Tour, J. M. Splitting of a Vertical Multiwalled Carbon Nanotube Carpet to a Graphene Nanoribbon Carpet and Its Use in Supercapacitors. *ACS Nano* **2013**, *7*, 5151–5159.

2. Lin, J.; Peng, Z.; Xiang, C.; Ruan, G.; Yan, Z.; Natelson, D.; Tour, J. M. Graphene Nanoribbon and Nanostructured SnO_2 Composite Anodes for Lithium Ion Batteries. *ACS Nano* **2013**, *7*, 6001–6006.

3. Li, Y.; Zhou, W.; Wang, H.; Xie, L.; Liang, Y.; Wei, F.; Idrobo, J.-C.; Pennycook, S. J.; Dai, H. An Oxygen Reduction Electrocatalyst Based on Carbon Nanotube−Graphene Complexes. *Nat. Nanotechnol.* **2012**, *7*, 394–400.

4. Zhu, Y.; Sun, Z.; Yan, Z.; Jin, Z.; Tour, J. M. Rational Design of Hybrid Graphene Films for High-Performance Transparent Electrodes. *ACS Nano* **2011**, *5*, 6472–6479.

5. Xiang, C.; Cox, P. J.; Kukovecz, A.; Genorio, B.; Hashim, D. P. Functionalized Low Defect Graphene Nanoribbons and Polyurethane Composite Film for Improved Gas Barrier

and Mechanical Performances. *ACS Nano* **2013**, *7*, 10380–10386.

6. Xiang, C.; Lu, W.; Zhu, Y.; Sun, Z.; Yan, Z.; Hwang, C-C.; Tour, J. M. Carbon Nanotube and Graphene Nanoribbon-Coated Conductive Kevlar Fibers. *ACS Appl. Mater. Interfaces* **2011**, *4*, 131–136.

7. Kosynkin, D. V.; Lu, W.; Sinitskii, A.; Pera, G.; Sun, Z.; Tour, J. M. Highly Conductive Graphene Nanoribbons by Longitudinal Splitting of Carbon Nanotubes Using Potassium Vapor. *ACS Nano* **2011**, *5*, 968–974.

8. Genorio, B.; Lu, W.; Dimiev, A. M.; Zhu, Y.; Raji, A.-R. O.; Novosel, B.; Alemany, L. B.; Tour, J. M. In Situ Intercalation Replacement and Selective Functionalization of Graphene Nanoribbon Stacks. *ACS Nano* **2012**, *6*, 4231–4240.

9. Lu, W.; Ruan, G.; Genorio, B.; Zhu, Y.; Novosel, B.; Peng, Z.; Tour, J. M. Functionalized Graphene Nanoribbons via Anionic Polymerization Initiated by Alkali Metal-Intercalated Carbon Nanotubes. *ACS Nano* **2013**, *7*, 2669–2675.

10. Cano-Márquez, A. G.; Rodríguez-Macías, F. J. Ex-MWNTs: Graphene Sheets and Ribbons Produced by Lithium Intercalation and Exfoliation of Carbon Nanotubes. *Nano Lett.* **2009**, *9*, 1527–1533.

11. Marcano, D. C.; Kosynkin, D. V.; Berlin, J. M.; Sinitskii, A.; Sun, Z.; Slesarev, A.; Alemany, L. B.; Lu, W.; Tour, J. M. Improved Synthesis of Graphene Oxide. *ACS Nano* **2010**, *4*, 4806–4814.

12. Kosynkin, D. V.; Higginbotham, A. L.; Sinitskii, A.; Lomeda, J. R.; Dimiev, A.; Price, B. K.; Tour, J. M. Longitudinal Unzipping of Carbon Nanotubes To Form Graphene Nanoribbons. *Nature* **2009**, *458*, 872–876.

13. Higginbotham, A. L.; Kosynkin, D. V.; Sinitskii, A.; Sun, Z.; Tour, J. M. Lower-Defect Graphene Oxide Nanoribbons from Multiwalled Carbon Nanotubes. *ACS Nano* **2010**, *4*, 2059–2069.

14. Bon, S. B.; Velentini, L.; Verdejo, R.; Garcia-Fierro, J. L.; Peponi, L.; Lopez-Manchado, M. A.; Kenny, J. M. Plasma Fluorination of Chemically Derived Graphene Sheets and Subsequent Modification with Butylamine. *Chem. Mater.* **2009**, *21*, 3433–3438.

15. Yazami, R.; Hamwi, A. Fluorination of Multi-layered Carbon Nanomaterials. U.S. Patent US7794880 B2, 2010.

16. Wang, Z.; Wang, J.; Li, Z.; Gong, P.; Liu, X.; Zhang, L.; Ren, J.; Wang, H.; Yang, S. Synthesis of Fluorinated Graphene with Tunable Degree of Fluorination. *Carbon* **2012**, *50*, 5403–5410.

17. Robinson, J. T.; Burgess, J. S.; Junkermeier, C. E.; Badescu, S. C.; Reinecke, T. L.; Perkins, F. K.; Zalalutdniov, M. K.; Baldwin, J. W.; Culbertson, J. C.; Sheehan, P. E.; Snow, E. S. Properties of Fluorinated Graphene Films. *Nano Lett.* **2010**, *10*, 3001–3005.

18. Mathkar, A.; Narayanan, T. N.; Alemany, L. B.; Cox, P.; Nguyen, P.; Gao, G.; Chang, P.; Romero-Aburto, R.; Mani, S. A.; Ajayan, P. M. Synthesis of Fluorinated Graphene Oxide and Its Amphiphobic Properties. *Part. Part. Syst. Charact.* **2013**, *30*, 266–272.

19. Jankovský, O.; Šimek, P.; Sedmidubský, D.; Matějková, S.; Janoušek, Z.; Šembera, F.; Pumera, M.; Sofer, Z. Water-Soluble Highly Fluorinated Graphite Oxide. *RSC Adv.* **2013**, *4*, 1378–1387.

20. Watanabe, N. Characteristics and Applications of Graphite Fluoride. *Physica B+C* **1981**, *105*, 17–21.

21. Gao, W.; Alemany, L. B.; Ci, L.; Ajayan, P. M. New Insights into the Structure and Reduction of Graphite Oxide. *Nat. Chem.* **2009**, *1*, 403–408.

22. Wang, X.; Dai, Y.; Gao, J.; Huang, J.; Li, B.; Fan, C.; Yang, J.; Liu, X. High-Yield Production of Highly Fluorinated Graphene by Direct Heating Fluorination of Graphene-Oxide. *ACS Appl. Mater. Interfaces* **2013**, *5*, 8294–8299.

23. Jeon, K.-J.; Lee, Z.; Pollak, E.; Moreschini, L.; Bostwick, A.; Park, C.-M.; Mendelsberg, R.; Radmilovic, V.; Kostecki, R.; Richardson, T. J.; Rotenberg, E. Fluorographene: A Wide Bandgap Semiconductor with Ultraviolet Luminescence. *ACS Nano* **2011**, *5*, 1042–1046.

24. Hamwi, A.; Daoud, M.; Cousseins, J. C. Graphite Fluorides Prepared at Room Temperature 1. Synthesis and Characterization. *Synth. Met.* **1988**, 89–98.

25. Palin, D. E.; Wadsworth, K. D. Structure of Carbon Monofluoride. *Nature* **1948**, *162*, 925–926.

26. Lei, Y. G.; Ng, K. M.; Weng, L. T.; Chan, C. M.; Li, L. XPS C 1s Binding Energies for Fluorocarbon−Hydrocarbon Microblock Copolymers. *Surf. Interface Anal.* **2003**, *35*, 852–855.

27. Gao, W. Graphite Oxide: Structure, Reduction and Applications. Ph.D. Thesis, Rice University, Houston, TX, 2012; http://www.dspace.rice.edu/handle/1911/64614.

28. Zhang, W.; Dubois, M.; Guérin, K.; Bonnet, P.; Kharbache, H.; Masin, F.; Kharitonov, A. P.; Hamwi, A. Effect of Curvature on C−F Bonding in Fluorinated Carbons: From Fullerene and Derivatives to Graphite. *Phys. Chem. Chem. Phys.* **2010**, *12*, 1388–1398.

29. Mallouk, T.; Hawkins, B. L.; Zilm, C. K.; Maciel, G. E.; Bartlett, N. Raman, Infrared and NMR Studies of the Graphite Hydrofluorides $C_xF_{1−\delta}(HF)_{\delta(2\leq x\leq 5)}$. *Philos. Trans. R. Soc. London, Ser. A* **1985**, *314*, 179–187.

30. Douwel, C. H. K.; Maas, W. E. J. R.; Veeman, W. S.; Buning, G. H. W.; Vankan, J. M. J. Miscibility in PMMA/PVF2 Blends, Studied by $^{19}F−^{13}C$ CPMAS NMR. *Macromolecules* **1990**, *23*, 406–412.

31. Eijkelenboom, A. P. A. M.; Maas, W. E. J. R.; Veeman, W. S.; Buning, G. H. W.; Vankan, J. M. J. Triple-Resonance Fluorine-19, Proton, And Carbon-13 CP-MAS NMR Study of the Influence of PMMA Tacticity on the Miscibility in PMMA/Poly(vinylidene fluoride) (PVF2) Blends. *Macromolecules* **1992**, *25*, 4511–4518.

32. Hagaman, E. W.; Burns, J. H. The Determination of Local Structure in Organofluorides Using Fluorine-19 Carbon-13 Dipolar Coupling. *Fuel* **1993**, *72*, 1239–1243.

33. Hagaman, E. W.; Lee, S. K. $^{19}F−^{13}C$ Cross Polarization 13C NMR: An Exploratory Study of Structure and Reactivity of Fluorinated Coal Using Elemental Fluorine. *Coal Sci. Technol.* **1995**, *24*, 339–341.

34. Hagaman, E. W.; Suk Kyu Lee, A.; Britt, P. F. Synthesis and Solid State ^{13}C and ^{19}F NMR Characterization of Aliphatic and Aromatic Carboxylic Acid Fluoride Polymers. *Anal. Chem.* **1997**, *69*, 3950–3958.

35. Holstein, P.; Scheler, U.; Harris, R. K. Triple-Channel Solid-State NMR Investigation of Poly(vinylidene fluoride) Polymorphs. *Magn. Reson. Chem.* **1997**, *35*, 647–649.

36. Nordon, A.; Harris, R. K.; Yeo, L.; Harris, K. D. M. Application of Triple-Channel $^{13}C\{^1H,^{19}F\}$ NMR Techniques To Probe Structural Properties of Disordered Solids. *Chem. Commun.* **1997**, 2045–2046.

37. Hagaman, E. W.; Murray, D. K.; Del Cul, G. D. Solid State ^{13}C and ^{19}F NMR Characterization of Fluorinated Charcoal. *Energy Fuels* **1998**, *12*, 399–408.

38. Ando, S.; Harris, R. K.; Hirschinger, J.; Reinsberg, S. A.; Scheler, U. Solid-State ^{19}F MAS, ^{19}F CRAMPS, and ^{19}F → ^{13}C CP/MAS NMR Study of an Amorphous Perfluoropolymer. *Macromolecules* **2001**, *34*, 66–75.

39. Vogt, F. G.; Vena, J. A.; Chavda, J. A.; Clawson, J. S.; Strhmeier, M.; Barnett, M. E. Structural Analysis of 5-Fluorouracil and Thymine Solid Solutions. *J. Mol. Struct.* **2009**, *932*, 16–30.

40. Karoyo, A. H.; Sidhu, P.; Wilson, L. D.; Hazendonk, P. Characterization and Dynamic Properties for the Solid Inclusion Complexes of β-Cyclodextrin and Perfluorooctanoic Acid. *J. Phys. Chem. C* **2013**, *117*, 8269–8282.

41. Soler, J. M.; Artacho, E.; Gale, J. D.; Garcia, A.; Junquera, J.; Ordejon, P.; Sanchez-Portal, D. The SIESTA Method for Ab Initio Order-*N* Materials Simulation. *J. Phys.: Condens. Matter* **2002**, *14*, 2745–2779.

42. Zhou, S.; Bongiorno, A. Density Functional Theory Modeling of Multilayer "Epitaxial" Graphene Oxide. *Acc. Chem. Res.* **2014**, *47*, 3331–3339.

43. Alemany, L. B.; Zhang, L.; Zeng, L.; Edwards, C. L.; Barron, A. R. Solid-State NMR Analysis of Fluorinated Single-Walled Carbon Nanotubes: Assessing the Extent of Fluorination. *Chem. Mater.* **2007**, *19*, 735–744.

44. Hayashi, S.; Hayamizu, K. Chemical Shift Standards in High-Resolution Solid-State NMR (1) ^{13}C, ^{29}Si, and ^1H Nuclei. *Bull. Chem. Soc. Jpn.* **1991**, *64*, 685–687.